Full-potential band-structure calculation of iron pyrite

I. Opahle
Institute of Theoretical Physics, TU Dresden, D-01062 Dresden, Germany

K. Koepernik
Max Planck Institute CPFS, D-01187 Dresden, Germany

H. Eschrig
IFW Dresden, P.O.B. 270016, D-01171 Dresden, Germany

(Received 1 June 1999)

Transition metal disulfides of pyrite structure have recently attracted much interest again due to their large variety of electronic, magnetic, and optical properties. The semiconductor iron pyrite (FeS_2) shows, for instance, an unusual blueshift of the optical gap under pressure. We present a full-potential total energy calculation of iron pyrite using density functional theory with a nonorthogonal local orbital minimum basis scheme. A sophisticated decomposition of the crystal potential and density into a lattice sum of local overlapping nonspherical contributions gives our approach a high numerical efficiency and makes it well suited for open structures like pyrite. For the decomposition of the exchange and correlation potential we introduced a technique of partitioning of unity based on Voronoi polyhedra. We obtain a sufficiently good agreement between our calculations and experimental values for the lattice constant, the positions of the sulfur atoms in the lattice, the bulk modulus, and the frequency of the A_g phonon mode to make a reliable study of the effect of isotropic external pressure on the electronic structure of pyrite and to obtain insight into the optical properties of pyrite. [S0163-1829(99)06843-5]

I. INTRODUCTION

Transition metal disulfides of pyrite structure have been in the interest of scientific research for a long time due to their large variety of electronic, magnetic, and optical properties. In this paper we will focus on the properties of the semiconductor iron pyrite FeS_2 with its promising capabilities for photovoltaic applications.[1,2]

Experimental data on the electronic structure of iron pyrite have been reported from numerous works, including photoelectron spectroscopy[3] and optical measurements of the band gap. The values for the optical band gap vary in a broad range from 0.7 eV to 2.62 eV. An overview is given in Refs. 4 and 5. Most reliable values are reported from photoconductivity measurements yielding values of approximately 0.9 to 0.95 eV. Data on the lattice structure and dynamics are available from x-ray diffraction,[6] ultrasonic measurements,[7] shock wave compression,[8] and Raman and infrared spectroscopy.[9–12]

Self-consistent band-structure calculations[13–18] of pyrite show quite a remarkable agreement. However, due to its open structure, pyrite is still a challenge for theoretical calculations of the electronic structure and the ground state energy. It was shown by Folkerts *et al.*[17] that when using a muffin-tin approximation, it is necessary to include so-called empty spheres in the calculation, and in the most recent calculation of Eyert *et al.*[16] the number of empty spheres in the unit cell was even increased to 32 before the results became stable. The pyrite structure has two structural degrees of freedom, namely the lattice constant a_0 and the Wyckoff parameter x_S determining the positions of the sulfur atoms in the unit cell. Theoretical values of these parameters were published by Zeng and Holzwarth,[13] who used a pseudopotential formalism within the frozen core approximation for their calculations. In their paper, they mainly focused on the valence electron distribution and cohesive energy comparing results of the local density approximation (LDA) and generalized gradient approximation (GGA) for the exchange and correlation potential. In a recent publication of Nguyen-Manh *et al.*[18] the equation of state and the reflectivity spectrum of iron pyrite under pressure were calculated using a tight-binding linear muffin-tin orbitals method.

Further theoretical studies of the influence of external pressure on the electronic structure have, to our knowledge, not been published yet and the understanding of this influence is still quite incomplete. Experimentally, it was found that the implantation of small amounts of Zn into FeS_2 ($<5\times10^{20}$ cm^{-3}) increases the optical gap by an amount of 0.07 eV.[16] In theoretical calculations, even a small change of the sulfur position in the lattice results in a drastic change of the band gap. On this basis, it was speculated that under application of external pressure, the compression of S-S bonds is larger than that of Fe-S bonds in order to explain the experimentally observed blueshift of the band gap.[9] This, however, is in contradiction to the experimental findings of Will *et al.*,[6] where a reduction of the sulfur parameter under application of external pressure is reported. In order to solve this contradiction, we determined the theoretical sulfur position for several lattice constants with our self-consistent full potential band-structure calculation scheme which will be discussed briefly in the next section. In Sec. III we present the results of our theoretical calculations for mechanical properties like lattice parameters, bulk modulus, and the A_g phonon mode. A discussion of the band structure and the

corresponding density of states for different external conditions gives a natural explanation for the experimental findings discussed above.

II. CALCULATIONAL SCHEME

A. General aspects

The full-potential nonorthogonal local-orbital minimum basis band-structure method used in this paper is described in detail elsewhere.[19] Here we focus on the main aspects of the scheme. The extended states are expressed as a linear combination of local orbitals. These orbitals are solutions to an atomlike Schrödinger equation in the spherically averaged crystal potential. The orbitals may be classified by virtue of their overlap. States from different sites, which do not overlap, are treated as core states. All other (mutually overlapping) states are valence states. The calculation of the valence states is modified by introducing an additional confining potential of the form $(r/r_0)^4$. It serves to compress the far ranging tails of the orbitals. This compression enhances the suitability of the valence basis orbitals for the band-structure calculation and raises the orbital energies, necessary for the description of scattering states. The compression radii have been shown in Ref. 20 to scale basically with the 3/2 power of the nearest-neighbor distance: $r_0=(x_0 r_{\mathrm{NN}}/2)^{3/2}$. The parameters x_0 are chosen to depend on the angular momentum l of the orbitals.

Consequently, the valence orbitals are no longer orthogonal even at the same site. The main advantage of the compression procedure is a high basis flexibility although the basis dimension is kept at its minimum value. A proper adjustment of the compression radii with respect to the minimization of the total energy gives an optimized basis set.

The density and the potential are represented by a lattice sum of local overlapping nonspherical contributions. The nonsphericity is taken into account by a spherical harmonics expansion of the local contributions up to a cut-off angular momentum $L_{\max}$. Due to the overlap of the local potentials, there is no shape restriction of the potential. We need no atomic spheres and therefore, we need no (time consuming) Fourier expansion for the interstitial potential.

The calculation of the density from the wave functions contains two types of expressions. The net density is formed of orbitals at the same site only and its lm decomposition is easily achieved. The overlap density is formed of orbitals at two different sites. To decompose this contribution into local parts centered at the corresponding sites, we employ a one-dimensional partitioning of unity along the axis joining the two sites.

From the density, the Hartree potential is easily calculated by means of the Poisson equation. The only potential contribution which does not properly fit to our local decomposition is the exchange and correlation (xc) potential. This nonlinear function of the density has to be decomposed into parts centered at the lattice sites and falling off rapidly while approaching the neighboring sites. In Ref. 19 we introduced a technique of partitioning of unity resulting in local shape functions. However, we realized that this definition, though generally valid, was not well suited for the present calculations, since the compact support of the resulting shape functions was rather elongated in certain directions. Thus, keeping the basic idea, we chose a new definition given in the next subsection.

B. The Voronoi shape functions

Our aim is to find a set of functions $f_s(\mathbf{r})$ with the property

$$\sum_{\mathbf{R}+\mathbf{s}} f_s(\mathbf{r}-\mathbf{R}-\mathbf{s})\equiv 1 \tag{1}$$

with $\mathbf{R}+\mathbf{s}$ being a lattice site with atom type s. Additionally, we demand that each function f_s has compact support Ω_s (the domain outside of which $f_s=0$) which excludes all lattice sites from its interior except the center. This implies $f_s(0)=1$. For the sake of applicability in band-structure calculations we further want the shape functions to have the symmetry properties of the underlying lattice. Especially in cases when there are large portions of empty space in the lattice, it is desirable to have the most ''isotropic'' support, since then the product of any function $v(\mathbf{r})$ with the shape function gives the most spherical result, reducing the number of lm components to be taken into account in a spherical harmonics expansion.

The last requirement is fulfilled by the Voronoi cells. They are defined in analogy to the Wigner-Seitz cell but for an arbitrary point set. The cell is the intersection of all closed half-spaces bounded by planes $\boldsymbol{\tau}\mathbf{r}/|\boldsymbol{\tau}|^2=1/2$, where $\boldsymbol{\tau}=\mathbf{R}+\mathbf{s}'-\mathbf{s}$ is a vector pointing from the center of the cell to any other site. In fact, only sites of some vicinity of the center site do contribute to the definition of the boundary. The Voronoi cells do not overlap, but for our purpose we need the compact supports from different sites to overlap. Thus we enlarge the cells by using an eight times larger cell with $\boldsymbol{\tau}\mathbf{r}/|\boldsymbol{\tau}|^2=1$.

Then we define a function

$$\tilde{f}_s(\mathbf{r})=\prod_{\{\boldsymbol{\tau}\}} h\left(\frac{\boldsymbol{\tau}\mathbf{r}}{|\boldsymbol{\tau}|^2}\right)$$

with $\mathbf{r}$ being the offset vector from the site s and with an auxiliary function having the property: $h(x)=1$ for $x\leqslant 0$ and $h(x)=0$ for $x\geqslant 1$. $\tilde{f}_s$ indeed fulfills all demands described above except for the unity condition Eq. (1). This, finally, is achieved by normalizing the shape function each time a value is needed

$$f_s(\mathbf{r})=\frac{\tilde{f}_s(\mathbf{r})}{\sum_{\boldsymbol{\tau}} \tilde{f}_{s'}(\mathbf{r}-\boldsymbol{\tau})}$$

where the sum runs effectively over all sites with $\Omega_s\cap\Omega_{s'}\neq\varnothing$ (including $\mathbf{s}=\mathbf{s}'$). This normalized function is not stored since it turned out that its numerical computation is fast enough.

The shape functions defined in this way are smooth functions which approach zero at the neighboring sites with any wanted power law due to the choice of $h(r)$. For a similar technique see, e.g., Becke.[21] However, the Becke functions do not have a compact support, which enlarges the domain from which the shaped potential is sampled.

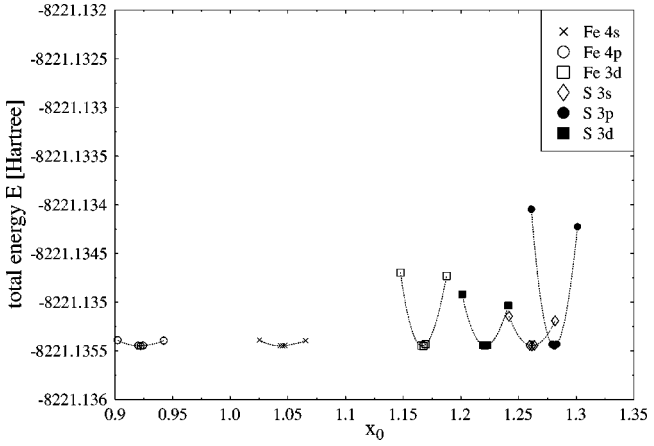

FIG. 1. Variation of the total energy with respect to the compression parameters x_0.

The set of sites defining the support Ω_s may be enlarged without changing Ω_s by adding shells of sites further away. Sometimes, when atomic positions in the unit cell shall be varied, the topology of the Voronoi cells depends on some position parameter. Then, one can construct cells which apply to all parameter values by just forming the union of the sets of vectors $\boldsymbol{\tau}$ for all parameter values.

C. Details of the present calculation

Our calculations are based on nonrelativistic density functional theory (DFT) in local density approximation (LDA) using the Perdew-Zunger parametrization[22] of the exchange and correlation potential of the homogeneous electron gas. As minimum orbital basis set we used Fe $4s$, $4p$, $3d$ orbitals and S $3s$, $3p$, $3d$ orbitals. In order to optimize our minimum basis, we varied the parameter x_0 of the confining potential introduced in the last section. The optimal choice of parameters minimizing the total energy are shown in Fig. 1. Since Fe $4s$ and $4p$ orbitals contribute only a little to the occupied band states, the total energy remains rather insensitive to the choice of x_0 for these orbitals. A change of the unit cell volume basically does not change the optimum set of x_0 parameters. However, a variation of the sulfur position in the unit cell leads to different x_0 parameters, and due to the relatively strong dependence of the total energy on these parameters, we had to adjust the set of parameters for these calculations.

In order to check the convergence of our results, we performed various calculations with increasing cut-off momentum L_{max}. The result is given in Fig. 2. The total energy varies less than 2 m Hartree per atom between $L_{max}=8$ and 12. (Note that L_{max} is not a variational parameter, hence the most accurate total energy result is not the lowest one.) For all that follows, a cut-off momentum of $L_{max}=12$ was used. Convergence with respect to the fineness of the **k** space grid was ensured by a sequence of calculations with an increasing number of 11, 24, 45, and 119 **k** points in the irreducible wedge of the Brillouin zone.

III. RESULTS AND DISCUSSION

A. Electronic structure using the experimental lattice parameters

Most of the calculations of the electronic structure published so far were done using the experimental lattice parameters. Except for Refs. 13 and 18, an optimization of the two free parameters of the pyrite structure with respect to the total energy has, to the authors' knowledge, not been published yet. In order to compare our own results to published calculations, we first calculated the electronic structure of FeS_2 using the experimental data for the lattice constant and sulfur positions.[6]

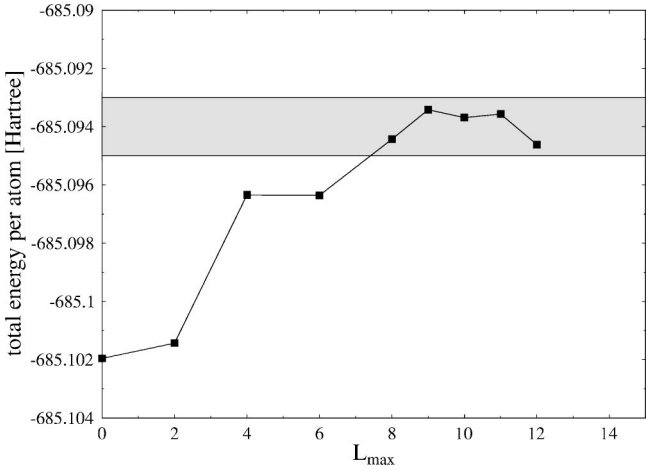

FIG. 2. Variation of the total energy with respect to the cut-off momentum L_{max}.

In Figs. 3 and 4 we show our calculated band structure of FeS_2 along selected high symmetry lines and the corresponding density of states. The agreement with the results of a recent calculation by Eyert *et al.*[16] is quite good. The band gap between occupied and unoccupied states is approximately 0.85 eV and coincides well with the experimental values of approximately 0.9–0.95 eV. However, we should mention that DFT in LDA usually does not give accurate values for the band gap of semiconductors.

The band structure is split into five groups of bands in the range between -18 eV and 5 eV relative to the valence-band maximum (VBM). The character of the bands can be evaluated using the partial density of states shown in Fig. 4. The two groups between -10 and -18 eV have almost entirely the character of S $3s$ states, which form bonding and antibonding subsets. The asymmetric shape of the corresponding

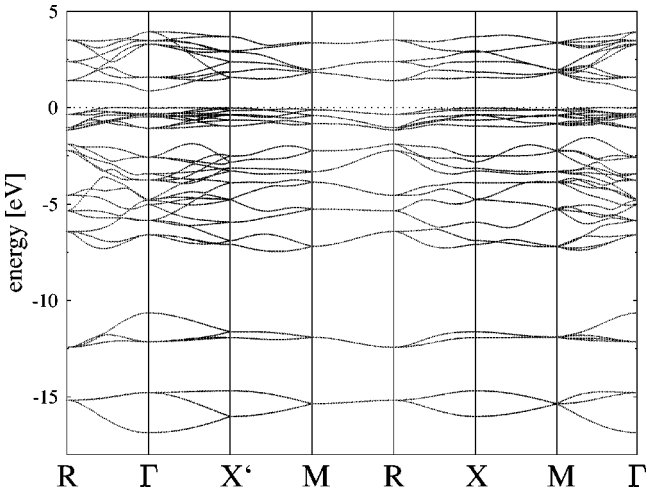

FIG. 3. Band structure of iron pyrite calculated with the experimental lattice parameters.

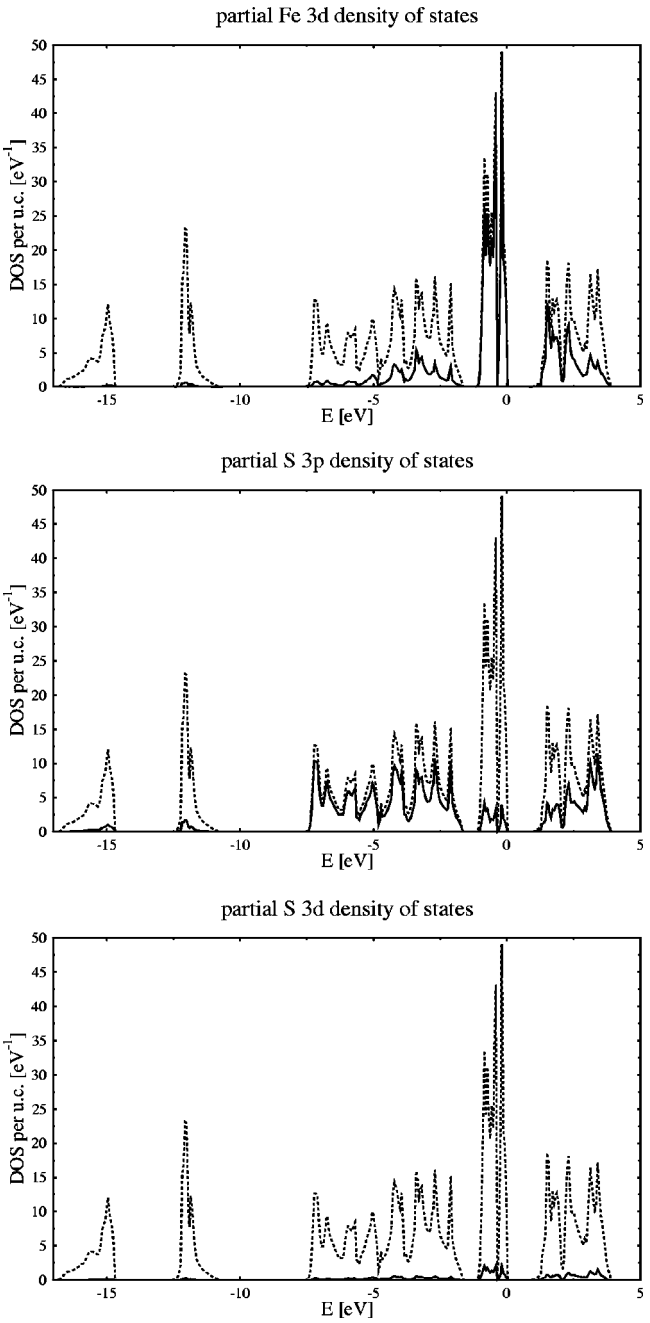

FIG. 4. Partial Fe $3d$, S $3p$, and S $3d$ densities of states of FeS_2 (solid lines) and total density of states (dashed lines) calculated with the experimental lattice parameters.

density of states was also found in previous calculations and is consistent with x-ray photoelectron spectroscopy (XPS) core level spectra of van der Heide *et al.*[3] who locate the $\sigma_g(3s)$ peak at -16.4 eV and the $\sigma_u^*(3s)$ peak at -13.3 eV. In comparison to Ref. 16, the S $3s$ bonding bands are shifted downwards by an amount of approximately 0.5 eV in our calculation, which is probably due to the different calculation schemes used, since bonding bands are more sensitive to the interstitial potential than antibonding bands. The next group of bands in the range between 7.5 and 1.5 eV below the VBM is formed of hybridized S $3p$ and Fe $3d$ states with the main contribution from S $3p$. The upper valence bands are formed of Fe $3d$ and S $3p$ states and some small admixture of S $3d$ with the main contribution from Fe $3d$. Finally, the

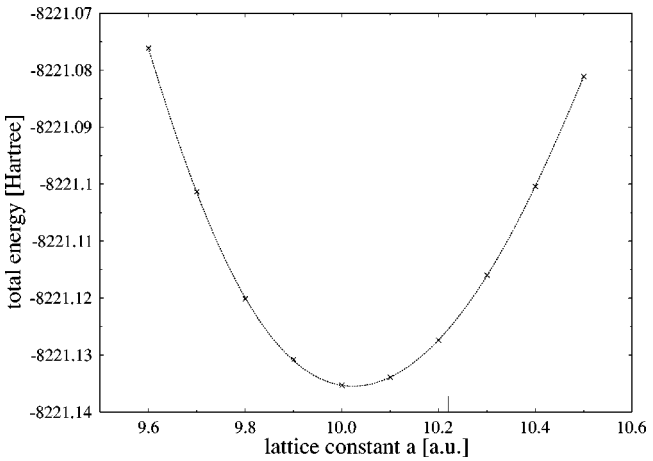

FIG. 5. Total energy vs. lattice constant a, calculated with the theoretical sulfur positions.

conduction band is formed mainly of hybridized Fe $3d$ and S $3p$ and $3d$ states. Fe $4s$ and Fe $4p$ states contribute mainly to the higher unoccupied bands not shown in Fig. 3. The band structure is discussed in more detail in Ref. 16.

B. Mechanical properties and influence of external pressure

Next, we want to study the influence of isotropic external pressure on the structure and properties of FeS_2. In Fig. 5 we show the variation of the total energy with respect to the lattice constant a. The theoretical value of the lattice constant $a_{theo}=10.02$ a.u. obtained by our calculations deviates from the experimental value $a_{exp}=10.22$ a.u.[6] by about 2% and is in good agreement with the calculated value of Nguyen-Manh *et al.*[18] The theoretical lattice constant obtained by Zeng and Holzwarth[13] was about 1% larger than the experimental value. Varying the position of the sulfur atoms in the lattice (see Fig. 6), we find a theoretical value of the Wyckoff parameter $x_S=0.377$, which is about 2% lower than the experimental value 0.386,[6] which means that in our calculation the bond length between neighboring sulfur atoms is enlarged. Similar results were also found in Refs. 13 and 18. From the total energy curve in Fig. 5 we obtained a value of 185 GPa for the bulk modulus $B=V(\partial^2 E/\partial V^2)$, which is

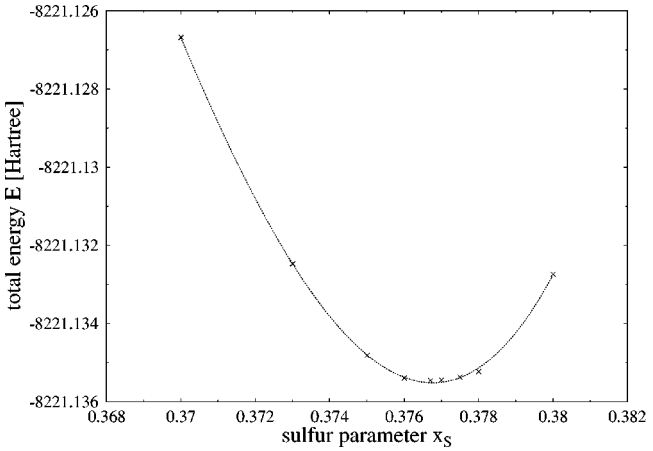

FIG. 6. Total energy vs. sulfur parameter x_S, calculated for the the theoretical lattice constant.

TABLE I. Comparision between experimental and calculated results.

	a (a.u.)	x_s	B (GPa)	$\hbar\omega_{A_g}$ (eV)
theoretical	10.02	0.386	185	0.48
experimental	10.22	0.377	145	0.54
deviation (%)	2	2	28	13

about 30% higher than the literature value $B=145$ GPa observed ultrasonically[7] and is in very good agreement with the calculated value $B=187$ GPa of Ref. 18. From other experimental methods bulk moduli between 118 GPa[6] and 162 GPa[8] are reported. The results are summarized in Table I together with the experimental values. Another interesting point is the effect of isotropic external pressure on the electronic structure of pyrite. A change of the sulfur Wyckoff parameter x_S has a considerably strong influence on the band structure of FeS_2. When varying x_S with a fixed lattice constant we find that the band gap becomes larger with increasing x_S, which was also found in Ref. 16. For the theoretical lattice parameters minimizing the total energy in our calculations, the band gap even vanishes (Fig. 7). A similar result was also found by Zeng and Holzwarth with their theoretical lattice and sulfur parameters. A change of the lattice constant results in a broadening of bands and rather does not influence the band gap. Assuming that the sulfur-sulfur bond compression is larger than that of Fe-S bonds when pyrite is exposed to external isotropic pressure, it was concluded in Ref. 16 that an increase of x_S can explain the experimental blueshift of the optical band gap observed by Batlogg as reported in Ref. 9. In Fig. 8 we show the total energy curves in dependence of the sulfur parameter x_S for different lattice constants. Although the exact determination of the minima of the curves is close to the limits of our numerical accuracy due to the shallow potential and the slight variation of the x_S parameter, the tendency of a decreasing x_S under external pressure is quite clear and was the same for all values of the lattice constant. Furthermore, this is in agreement with the experimental data of Will *et al.*[6] Thus, the scenario outlined in the paper of Eyert *et al.* cannot be the right explanation

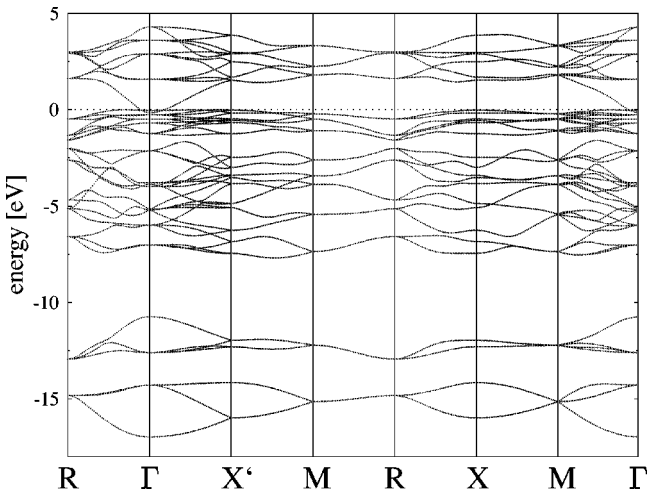

FIG. 7. Band structure of FeS_2 calculated for the theoretical lattice parameters minimizing the total energy.

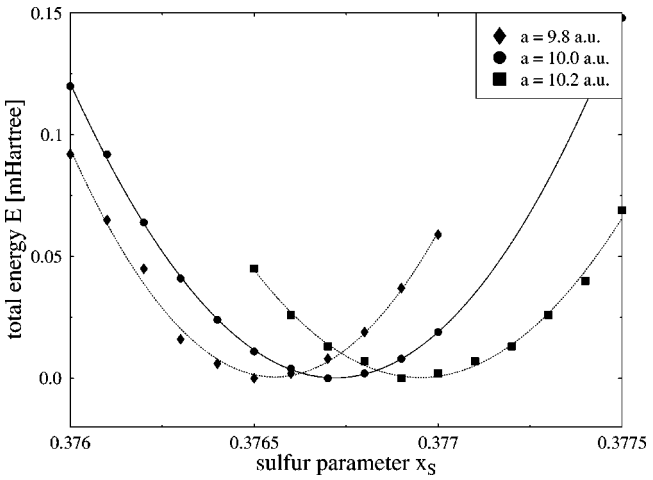

FIG. 8. Total energy in dependence of the sulfur parameter for different lattice constants. Energies are relative to the minimum of each lattice constant.

and the question why there is a blueshift of the optical band gap when pyrite is exposed to pressure remains to be answered. The picture becomes clearer if one takes a look at the overall behavior of the density of states for different pressures (Fig. 9). The steep band near the Γ point that causes the reduction of the band gap only contributes to a very shallow tail in the density of states, while the steep absorption edge for transitions into the antibonding Fe $3d$ and S $3p$ states is slightly shifted towards higher energies. Simultaneously, the bonding S $3p$ and Fe $3d$ band complex below -2 eV is shifted towards lower energies, clearly indicating that both shifts are caused by an increase in Fe-S covalency under pressure due to the reduction of the Fe-S bond length. For optical absorption measurements, we would finally expect that the increase of the absorption edge is measured. From our calculations we would expect a different behavior of the band gap in photoconductivity and optical absorption measurements, which would be an interesting experimental check of our results.

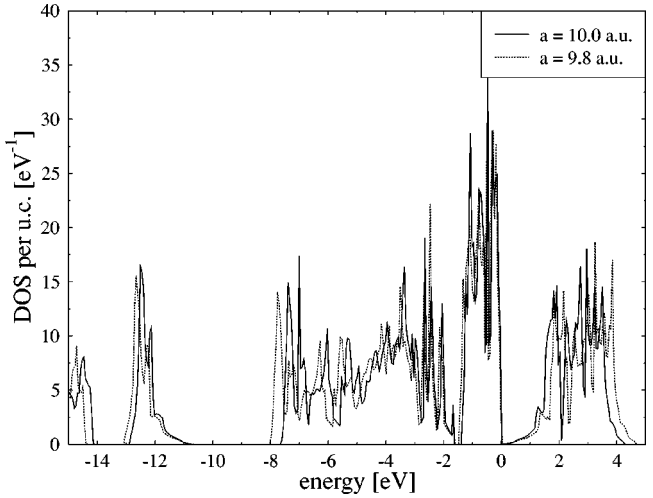

FIG. 9. Comparison between the total density of states for the lattice constants $a=10.0$ a.u. and $a=9.8$ a.u. with optimized sulfur parameters.

C. Calculation of the A_g-phonon mode

As a final check for the reliability of our results, we calculated the frequency of the A_g-phonon mode at the center of the Brillouin zone corresponding to the displacement of the sulfur atoms with variation of x_S. In the harmonic approximation, the Hamiltonian for the lattice vibrations is

$$H=\sum_{msi}\frac{p_{msi}^2}{2}+\frac{1}{2}\sum_{msi}\sum_{ntj}u_{msi}C_{ntj}^{msi}u_{ntj}, \tag{2}$$

where u_{msi} is the ith coordinate of the displacement of the atom s in the unit cell associated with the lattice vector $\mathbf{R}_m$ and $C_{ntj}^{msi}=\delta^2V(0)/\delta x_{msi}\delta x_{ntj}$ are the atomic force constants.

For the rth normal mode with wave vector $\mathbf{q}$, the atomic displacements are given by

$$u_{msi}=\frac{1}{\sqrt{NM_s}}e^{i\mathbf{q}\mathbf{R}_m}e_{si}^{(r)}Q_r(\mathbf{q}). \tag{3}$$

For the Γ point of the Brillouin zone, there are obvious simplifications for the classification of normal modes with respect to space group representations. For pyrite, the factor group is isomorphic to the the point group T_h and the normal modes have the following irreducible representations:[9]

$$A_g+E_g+3T_g+2A_u+2E_u+6T_u. \tag{4}$$

Since the vibration associated with a variation of x_S is invariant under all symmetry operations, it corresponds to the trivial A_g representation. For this mode, the normal coordinate is given by

$$Q=\sqrt{24NM_S}a\,\delta_S, \tag{5}$$

where a is the lattice constant and δ_S is the variation of the Wyckoff parameter x_S. From the relation

$$V(\delta_S)=\frac{1}{2}\omega^2Q^{\dagger}Q=12\omega^2a^2\delta_S^2NM_S=N\alpha\delta_S^2, \tag{6}$$

where α is obtained by a least squares fit to the data of Fig. 6, we get a value of $\hbar\omega=0.048$ eV for the energy of the A_g phonon mode. Experimentally, the Raman spectrum of pyrite shows one peak at the energy 0.054 eV which is believed to correspond to the A_g phonon mode.[12] Thus, also here we obtain good agreement between our calculations and experiment.

IV. CONCLUSION

In the present work we investigated the properties of iron pyrite by means of total energy calculations. Our full-potential method with a strictly local representation of all functions allowed us for accurate and numerically efficient calculations without use of empty spheres. The calculated lattice constant and sulfur parameter, bulk modulus, as well as the frequency of the A_g phonon mode are in a typical LDA agreement with experimental values. The calculated band structure is consistent with recent calculations and shows a nice agreement with experimental XPS spectra.

As in previous calculations, the band gap shows a strong correlation to the sulfur Wyckoff parameter x_S and is reduced with decreasing x_S. The drastic effect of the sulfur position on the band gap can at least partially explain the strong influence of impurities on the optical properties. Our total energy calculations show that the blueshift of the optical gap of pyrite under pressure cannot be attributed to a larger compression of S-S bonds in comparison to that of Fe-S bonds. We find the opposite effect, i.e., the x_S is decreased under pressure in agreement with experiment. However, the steep band near the Γ point that is responsible for this reduction contributes only to a very shallow tail in the density of states, while the absorption edge between occupied nonbonding Fe $3d$ states and unoccupied hybridized Fe $3d$–S $3p$ states is slightly shifted towards higher energies due to an increase in Fe-S covalent bonding strength. Thus, we conclude that the blueshift in absorption measurements under pressure can be attributed to this pseudogap behavior.

ACKNOWLEDGMENTS

One of the authors (H.E.) benefited from discussions with V. Eyert on the subject. This work was supported by Deutsche Forschungsgemeinschaft, SFB 463, TP B2.

[1] M. Birkholz, S. Fiechter, A. Hartmann, and H. Tributsch, Phys. Rev. B **43**, 11 926 (1991).
[2] A. Ennaoui, S. Fiechter, W. Jaegermann, and H. Tributsch, J. Electrochem. Soc. **133**, 97 (1986).
[3] H. van der Heide, R. Hemmel, C. F. van Bruggen, and C. Haas, J. Solid State Chem. **33**, 17 (1980).
[4] A. Ennaoui, S. Fiechter, Ch. Pettenkofer, N. Alonso-Vante, K. Büker, M. Bronold, Ch. Höpfner, and H. Tributsch, Sol. Energy Mater. Sol. Cells **29**, 289 (1993).
[5] I. J. Ferrer, D. M. Nevskaia, C. de las Heras, and C. Sanchez, Solid State Commun. **74**, 913 (1990).
[6] G. Will, J. Lauterjung, H. Schmitz, and E. Hinze, in *High Pressure in Science and Technology*, edited by C. Homan, R. K. MacCrone, and E. Whalley, Materials Reserach Society Symposia Proceedings No. 22 (Elsevier, New York, 1984), p. 49.
[7] R. Blachnik, S. Kovitnik, O. Steinmeier, A. Wilke, A. Feltz, H. Renter, and E. Stieber, *D'Ans-Lax, Taschenbuch für Chemiker und Physiker, Band III* (Springer, Berlin, 1998),
[8] T. J. Ahrens and R. Jeanloz, J. Geophys. Res. **92**, 10 363 (1987).
[9] A. Schlegel and P. Wachter, J. Phys. C **9**, 3363 (1976).
[10] H. D. Lutz, P. Willich, and H. Haeuseler, Z. Naturforsch. A **31A**, 847 (1976).
[11] H. D. Lutz and P. Willich, Z. Anorg. Allg. Chem. **405**, 176 (1974).
[12] H. H. Eysel, H. Siebert, and G. Agiorgitis, Z. Naturforsch. B **24B**, 932 (1969).

[13] Y. Zeng and N. A. W. Holzwarth, Phys. Rev. B **50**, 8214 (1994).
[14] W. M. Temmerman, P. J. Durham, and D. J. Vaughan, Phys. Chem. Miner. **20**, 248 (1993).
[15] G. L. Zhao, J. Callaway, and M. Hayashibara, Phys. Rev. B **48**, 15 781 (1993).
[16] V. Eyert, K.-H. Höck, S. Fiechter, and H. Tributsch, Phys. Rev. B **57**, 6350 (1998).
[17] W. Folkerts, G. A. Sawatzky, C. Haas, R. A. de Groot, and F. U. Hillebrecht, J. Phys. C **20**, 4135 (1987).
[18] D. Nguyen-Manh, D. G. Pettifor, H. M. Sithole, P. E. Ngoepe, C. Arcangeli, R. Tank, and O. Jepsen, in *Tight-Binding Approach to Computational Materials Science*, edited by P. E. A. Turchi, A. Gonis, and L. Colombo, Materials Research Society Symposia Proceedings No. 491 (Materials Research Society, Pittsburgh, 1998), p. 401.
[19] K. Koepernik and H. Eschrig, Phys. Rev. B **59**, 1743 (1999).
[20] H. Eschrig, *Optimized LCAO Method and the Electronic Structure of Extended Systems* (Springer, Berlin, 1989).
[21] A. D. Becke, J. Chem. Phys. **88**, 2547 (1988).
[22] P. Perdew and A. Zunger, Phys. Rev. B **23**, 5048 (1981).